

AN ALL SKY TRANSMISSION MONITOR: ASTMON

J. ACEITUNO¹, S.F SÁNCHEZ¹, F. J. ACEITUNO², D. GALADÍ-ENRÍQUEZ¹, J.J. NEGRO³, R.C. SORIGUER³, G. SANCHEZ GOMEZ⁴

Draft version October 22, 2018

ABSTRACT

We present here the All Sky Transmission MONitor (ASTMON), designed to perform a continuous monitoring of the surface brightness of the complete night-sky in several bands. The data acquired are used to derive, in addition, a subsequent map of the multiband atmospheric extinction at any location in the sky, and a map of the cloud coverage. The instrument has been manufactured to afford extreme weather conditions, and remain operative. Designed to be fully robotic, it is ideal to be installed outdoors, as a permanent monitoring station. The preliminary results based on two of the currently operative units (at Doñana National Park - Huelva- and at the Calar Alto Observatory - Almería -, in Spain), are presented here. The parameters derived using ASTMON are in good agreement with previously reported ones, what illustrates the validity of the design and the accuracy of the manufacturing. The information provided by this instrument will be presented in forthcoming articles, once we have accumulated a statistically amount of data.

Subject headings: Astronomical Phenomena and Seeing

1. INTRODUCTION

The night sky brightness, the number of clear nights, the seeing, transparency and photometric stability are some of the most important parameters that qualify a site for front-line ground-based astronomy (Taylor et al. 2004). There is limited control over all these parameters, and only in the case of the sky brightness is it possible to keep it at its natural level by preventing light pollution from the immediate vicinity of the observatory (Garstang 1989). Previous to the installation of any observatory, extensive tests of these parameters are carried out in order to find the best locations, maximizing then the efficiency of these expensive infrastructures (Thomas-Osip et al. 2010, Schock et al. 2009) . However, most of these parameters are not constant along the time, neither in short term nor in long term time scales.

An on-line monitoring of all these conditions has been proved to be a fundamental tool to take decisions on the observational strategies, in order to increase the efficiency of any professional observatory (Travouillon et al. 2011). In particular, a very interesting input to decide about the optimal strategy would be to estimate in real-time the stability of the atmosphere and the location of the darkest and the most transparent areas in the sky (eg, Benn & Ellison et al. 1998a,b; Sánchez et al. 2007; Moles et al. 2010; High et al. 2010; Zou et al. 2010).

Along the 26 years of operations of the Calar Alto observatory, there has been different attempts to characterize some of the main properties described before: (i) Leinert et al. (1995) determined the sky brightness corresponding to the year 1990; (ii) Hopp & Fernandez (2002) studied the extinction curve corresponding to the years

1986-2000; However, we lack of a consistent study of all of them, spanning over a similar time period. This information becomes even more important for long-term surveys, where automatic or semi-automatic schedulers are programmed in order to optimize the observation over large areas in the sky (eg., Moles et al. 2008).

In order to characterize these parameters most of the professional observatories have installed permanent monitors which provide an almost real-time estimation of them. The values produced by these monitors are frequently accessible on-line via web services, stored in databases, and even included in the headers of the images obtained at the observatory. They compose an extremely useful database on the long term stability of the night-sky conditions at a certain site. In general, most of these monitors produce global parameters, based on large aperture measurements, like the cloud monitors based on the temperature difference between the ground layer and the sky, or local parameters, like the information provided by most of the seeing and transparency monitors: eg., RoboDIMM (Aceituno 2004) or EXCALIBUR (Sánchez et al. 2007, Moles et al. 2010). On other occasions, all sky monitors provide qualitative estimations on the sky transparency, based on direct images to estimate the cloud coverage, but no quantitative ones.

As part of a large program to determine the observing conditions at different locations in Spain (Sánchez et al. 2007, 2008; Moles et al. 2010), we developed a new set of instruments, able to estimate the most important parameters that determine the quality of an astronomical site, working in fully automatic mode. The first of these instruments was named EXCALIBUR (Pérez-Rámirez et al. 2008), a multi-wavelength extinction monitor, whose main purpose was to determine the atmospheric attenuation curve, and derive the relative contribution of each its components, at a particular location in the sky. The main idea behind this instrument was to determine these parameters at the sample position where the astronomical observation is taking place, monitoring any possible

aceitun@caha.es

¹ Centro Astronómico Hispano-Alemán (CAHA A.I.E), Jesús Durbán Remón 2-2, 04004 Almería, Spain

² Instituto de Astrofísica de Andalucía (IAA), Consejo Superior de Investigaciones Científicas (CSIC), C/ Camino Bajo de Huétor 50, E-18008, Granada, Spain

³ Estación Biológica de Doñana, CSIC

⁴ SATEC

change in the night-sky stability.

This instrument provides accurate local information, but it cannot provide simultaneous information on the considered parameters at different locations in the sky. For doing so, a different concept of instrument is required. In this article we present the All Sky Transmission MONitor (ASTMON), an instrument that, working on the same principals of EXCALIBUR, derives the surface sky brightness, atmospheric extinction and extinction curve at several locations in the sky simultaneously. It also provides additional information about the night-sky quality, based on the measurements acquired, like the photometric conditions, cloud-coverage and amount of light-pollution.

Although the main goal of these instruments is to determine the night-sky quality for the astronomical observation, this information has been found useful in another science fields. Due to that, a prototype of an EXCALIBUR unit was installed in the Andalusian Center of Environment Studies (Granada), to estimate the light pollution and aerosol content in populated areas (Pérez-Ramírez et al. 2008). In addition, the first prototype of ASTMON was installed permanently in the Doñana Biological Reserve, CSIC (Spain), to determine the effects of the light pollution in the biological environment of this protected area. Both instruments were calibrated at the Calar Alto observatory, which has acquired and installed units of both of them, integrating them in their monitor systems. The calibration runs demonstrated that these instruments are able to provide quantitative valuable measurements in a completely automatic way, comparable to the values provided by other monitors and/or guided astronomical observations.

The structure of this article is as follows: in Section 2 we present the basic concepts in which the instrument is based; in Section 3 the instrument itself is described, illustrating its main components; in Section 4 we present the results from the calibration run, comparing them with those derived by other well tested monitors and/or published data. In Section 5, we present a summary of the results from the experiment and the future perspective of this kind of instruments.

2. BASIC CONCEPTS OF THE INSTRUMENT

The procedures adopted to derive the extinction and night-sky surface brightness for this instrument are based on simple photometric concepts (Falchi 2010). The first step consists of the acquisition of a full sky frame at a particular optical band, by the techniques that will be described below. The exposure time should be large enough to sample the sky-brightness in the areas free of objects with enough signal-to-noise ratio to derive a reliable measurement, and, at the same time, short enough not to saturate a sufficient number of bright stars, that are used as photometric self-calibrators.

A source detection algorithm is then run over the considered image, providing a catalogue of the stars detected in the field. Adopting an a-priori calibrated distortion solution, the catalogue of detected stars is cross-matched with an astrometric and photometric calibrated catalogue of stars. This procedure allows both to identify the stars and to estimate the corresponding airmass within the considered image. Then, the flux corresponding to each of these stars is derived by adopting a simple aper-



FIG. 1.— The figure shows an external view of an ASTMON unit. The internal components are protected by a weather - proof housing, so the instrument can be installed out-doors.

ture photometry algorithm on the image. The contribution from the sky emission is estimated by measuring the mode of the counts within a predefined annular ring around each star, correcting for the aperture differences, and subtracted to the flux measured in the central aperture. Different experiments have shown us that the mode is the most optimal statistical estimator of the surface brightness of the sky-background, when dealing with crowded fields and large pixel scales.

The described procedure provides us with a catalogue of detected stars. For each of them, the catalogue includes the coordinates of the star projected on the sky, its airmass, its calibrated photometry at the considered band, and the observed flux (in counts). These catalogues can be used to derive the instrumental zero-point (ZP) and the extinction coefficient for the considered band (κ), applying the following classical formulae:

$$2.5\log_{10}(F/t) + mag = ZP - \kappa * \chi \quad (1)$$

where F is the number of counts derived for the central aperture, t is the exposure time, mag is the catalogued magnitude for the considered star, and χ is the air-mass of the observed star. The extinction, that depends on the particular atmospheric conditions, is highly variable. However, the zero-point, that depends mostly on the characteristics of the instrument, is more stable with time. Under photometric conditions, in which the extinction coefficient is uniform at almost any location in the sky, it is possible to derive both parameters by performing a classical linear square-regression between the instrumental magnitude ($2.5\log(F/t) + mag$) and the airmass (χ). The wide airmass range covered by the instrument, allows to obtain an accurate estimation of both parameters with a single image. Although night-length photometric conditions are scarce, it is relatively easy to find short periods of photometric conditions, and therefore, it is possible to obtain several estimations of the zero-point in any clear night.

Once obtained the zero-point, the extinction is derived at each location in the sky, by solving the previous equation for κ . In addition to that, for each area free of targets it is possible to derive the sky-surface brightness,



FIG. 2.— The figure shows the internal view of the system: (1) Ground fault and electrical breakers. (2) Main fan. (3) Anti-humidity system. (4) CCD head with filter wheel. (5) Servo-motor of the solar shutter. (6) Servomotor controller. (7) Thermostats. (8) Main stabilized power supply. (9) PIC I/O controller. (10) Computer. (11) Acrylic dome.

by applying the formulae:

$$SB = ZP - 2.5 \log_{10}(F_{sky}/A) \quad (2)$$

where SB is the night-sky surface brightness in $\text{mag}/\text{arcsec}^2$, ZP is the zero-point at the considered band and F_{sky} is the number of counts per second measured in a certain area A (in square arcsec). This later parameter is the only one that presents a certain difficulty, since in all-sky monitors the area covered by each pixel is not uniform, and therefore an accurate area correction has to be applied, based on the estimation of the field distortion.

3. DESCRIPTION OF THE INSTRUMENT

3.1. The hardware

The technical design of the instrument is rather simple. It comprises (1) a fisheye to sample the full sky ($\sim 180^\circ$) in a single shot; (2) a filter-wheel, where the optical-band filters are located; (3) a CCD detector, including a shutter; (4) a electronics system that controls the different behaviors of the instrument and (5) a control and storage computer (a standard Core-Duo based laptop). All

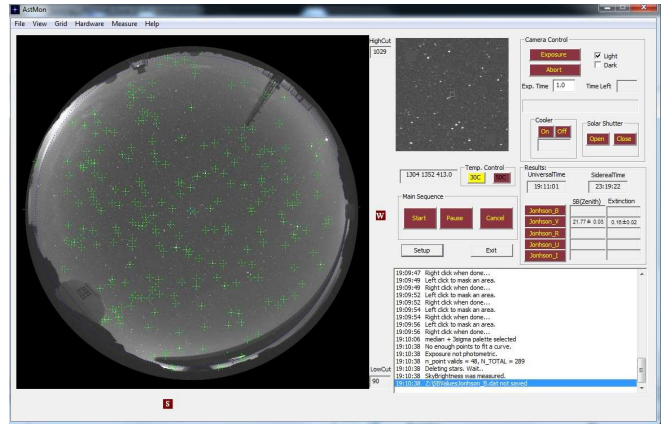


FIG. 3.— Snap-shot of the custom software developed for ASTMON, taken during one of the calibration runs. Different control buttons, entries, and panels showing the status of the instrument are seen at the right-side of the program. The panel at the left side shows one particular image of the night-sky. The green circles indicate the location of the detected stars that match with the corresponding ones at the astrometric/photometric catalogue, as described in the text.

the elements are packed in a enclosure prepared to afford extreme weather conditions.

Figure 1 shows an out-side view of the instrument, at the Calar Alto labs. The white enclosure has its front door open, and the control computer is seen, and the glass closing window on top of the light entrance. A solar shutter is placed just above the fisheye lens to protect it against the direct exposure to the sunshine. As indicated before, the enclosure is designed to afford extreme weather conditions, providing an almost isolated environment when it is closed. It is equipped with double isolated walls, and a drying system based on Chloride Calcium that keeps the humidity inside at about of 50-60% (ie., the optimal one to operate the electronics and CCD). The design maintains the instrument operational under high relative external humidities (near 100%), and prevents from any damage the internal cabling and components.

The imaging system consists of a fisheye lens that provides a field of view of 180 degrees, covering the full sky, and a camera. The camera mounts a KODAK KAF-8300 CCD of 8.3 megapixels, with tiny 5.4 microns pixels (figure 2). This results in a pixel scale of 3.8 arcminutes per pixel. A filter-wheel, with 5 different holders, is located between the fisheye lens and the camera. A set of standard Johnson filters is used, included U, B, V, R and I for the Calar Alto unit and B, V and I for the Doñana unit. However any set of filters that matched the holders (1 1/4 inches diameter), can be installed if required.

The temperature within the enclosure is sampled by four sensors, installed at different locations. If the temperature rises to a critical value (due to the combined heating of the CCD, electronics and computer), and automatic fan activates to extract the hot air through a pipe designed for this purpose. This pipe includes a system to avoid that rain or snow gets into the enclosure. On the other hand, if the temperature drops below a critical value, a heating system is activated. The whole system forces the temperature to be stable within a range of optimal values, under any external conditions. In addition to that, an humidity sensor monitors the value of the

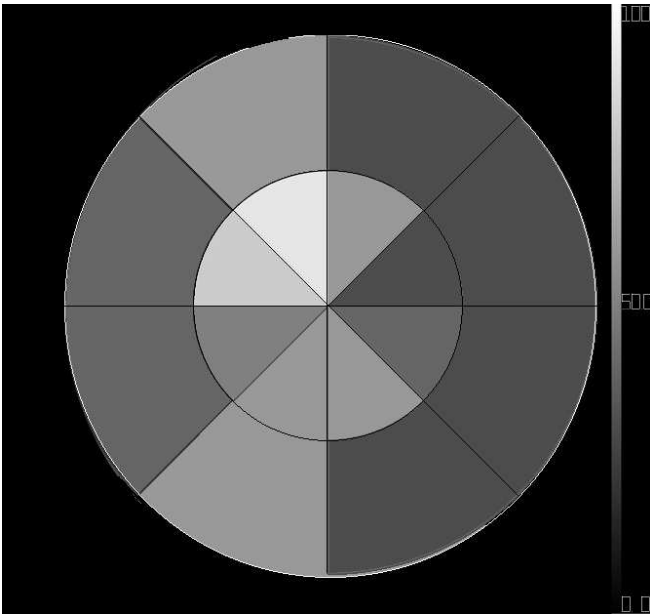


FIG. 4.— Map of the clouds coverage generated by ASTMOM during a mildly cloudy night at the Doñana National Park. The greycolor scale represents the percentage of cloud's coverage, where the darker regions correspond to the clearer sky areas.

current internal humidity, and disconnects the system if a critical value is reached.

The main electronics comprise an USB relay board and a set of digital/analog inputs based on a micro-pic controller. This system allows the computer to take control on the internal power of all the devices. In this way it is easy to deactivate the system during day time and to reactivate it again when the sun is set. The electronics comprises too a servo motor controller for the solar shutter and 4 analog inputs to read the values of the temperature sensors described before. Finally, a ground fault and electrical breakers have been included for security.

Figure 2 shows the interior of the instrument, from the main door towards the inside of the enclosure. The different elements described before have been labelled, illustrating their location within the system.

3.2. The software

3.2.1. Control system and starting up

The electronics of the system are controlled by the computer through a custom designed software, which allows the instrument to be completely robotic. The software switches on the system on the basis of the computers time and date, by checking if the astronomical night has started. In a similar way, it switches off the system, when the astronomical night has gone. To switch on the system, the computer activates all the powers and enables the communication between the CCD and the filter wheel. Then, it activates the cooling system of the CCD, in order to reach the optimal operational temperature of -15° Celsius. Once this temperature is reached, the program generates a master bias by taking a set bias frames, and getting the median. Dark current is particularly high for this particular CCDs. In order to remove this from the science frames, a set of dark frames with different integration times is derived, and stored, during the startup procedure. In this way, it is not needed to take a dark frame for each science observation.



FIG. 5.— Picture of DomeLight. This device has been developed to shine uniformly any wide-field camera.

Once performed the startup procedure, the program starts the acquisition of data, following a predefined sequence. Each step in the sequence comprises the selection of a certain filter, the acquisition of a set of images, and their reduction and analysis. The only parameter to be adjusted of these sequence is the exposure time of the frames taken with each filter. The final selected exposure times are 300 seconds for the U-band and 40 seconds for remaining ones (B,V,R and I). These values were derived experimentally, driven by the compromise between taking exposures short enough not to be affected by the rotation of the Earth (which affects to the astrometric solution and the shape of the stars on the images), and getting, on the other hand, enough signal-to-noise ration in both the stars and the night-sky background. The data are corrected for the bias and master dark immediately after acquiring them. After that, a master flatfield correction is applied (we will describe later how it is obtained). Finally, a mask is applied to remove from the images any artifact due to local buildings, trees, and so on. This mask is generated manually, by a routine included in the software. This procedure has to be done only once, when the instrument is operated for the first time at a particular location.

3.2.2. Astrometric solution.

Once a particular frame is obtained for a particular band, and the data are reduced, the program starts to analyze it. First, it performs an automatic identifications of the stars in the image. The program uses the Ducati (2002) photometric catalog, that comprises of accurate astrometric positions and photometry for most of the stars down to 6th magnitude in all the Johnson bands. However, any other catalogue can be selected by the user, by simply marking it in the program interface.

Fisheye lenses suffer from strong geometric optical aberrations, that have to be corrected prior to finding the astrometric solution. The correction required for the geometric aberration is derived empirically, being required to be obtained only once, during the calibration runs of the the instrument. For deriving this calibration the software includes a routine that allows to display on top of the acquired night-sky image the theoretical positions of a hundred of stars in the field of view. Then, the

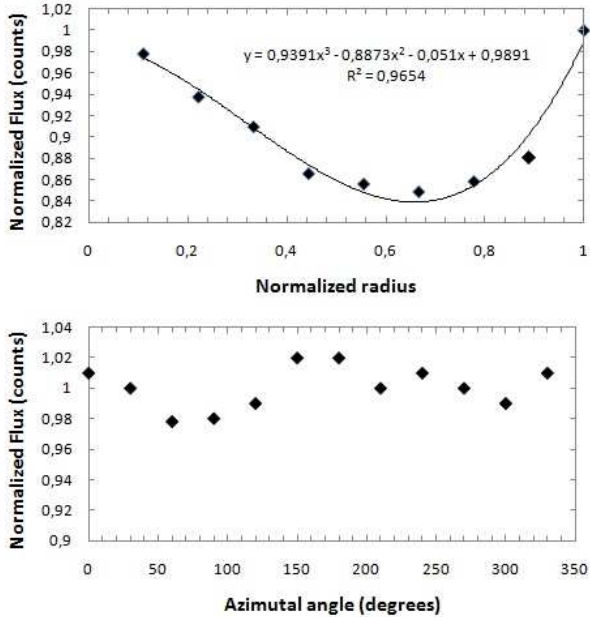


FIG. 6.— Estimation of the illumination correction of the DomeLight device. The top panel shows the radial distribution of the intensity measured with the two apertures sensor, and the bottom panel shows the azimuthal one. In both cases the intensity is normalized to the intensity at the zenith. The solid line in the left panel shows the best fitted 2nd order polynomial function.

user is requested to match the estimated and real positions of the stars within the field, by clicking on them. The coordinates of this manual selection are used as a first approximation to the final ones. Those are derived on the basis of an automatic centroid algorithm, which looks for the brightest star within a diameter of 8 pixels (30 arcminutes) with respect to the manually selected coordinates. When more than one bright star is found, they are discarded from the final catalogue. Fortunately the probability of getting several stars brighter than 6th magnitudes in a region of 30 arcminutes is low. The adopted centroid procedure has an accuracy of ~ 1 pixel (3.75 arcminutes), sufficient for its purpose.

After this matching process, the software evaluates the radial optical aberration of the fisheye by fitting a second order polynomial function to the differences between the estimated and observed positions with respect to the radial distance. This solution is stored to be applied as part of the astrometric solution to the images.

3.2.3. Diagram of the coverage by clouds

As a result of the plate solution, a cloud map is generated for each acquired frame. To derive this cloud map, the sky image is divided in 16 areas, following the pattern shown in Figure 4. The number of detected stars is compared with the number of expected (on the basis of the considered catalogue), within each of these areas. The ratio between both parameters is used as an estimation of the cloud coverage, assuming that stars are not detected due mostly to the presence of clouds. The program represents the final cloud-coverage diagram as a grayscale image, where the darker sectors represent the areas of larger percentage of sky without clouds (Fig-

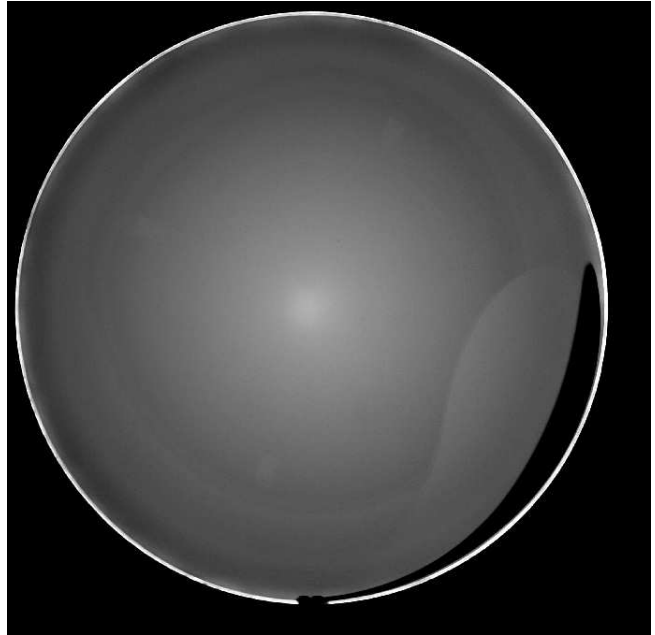


FIG. 7.— Flat field frame obtained with DomeLight in the V-band. The effect of the solar shutter is shown in the image. This effect also appears in the sky frames but it is corrected by the flat fields.

ure 4). Altogether the procedure provides a method to quantify the clouds's coverage.

3.2.4. Map of the night sky surface brightness

A classical aperture photometry is applied to each star detected in the field, by measuring the counts within a circle with a radius of 3 pixels, and two adjacent rings enclosed by circles with a radius of 4 and 6 pixels, respectively. The actual size of these radii can be modified by the user. According to Equation 1, the estimated extinction for all the stars is derived. Previously, the instrumental Zero Point has been calculated during a calibration run.

Afterwards, the stars are removed from the images by replacing the values of the intensity of the corresponding pixels by the mode intensity within the surrounding ones (Parker 1991). This cleaning procedure is adopted to avoid the contamination due to these sources. Finally, the night-sky brightness is derived for each pixel on the basis of equation 2. The final frame is stored as both FITS and JPEG files, which will allow the user to perform both further analysis and/or display the results in webpages or to produce movies with the provided information.

The software allows the user to define a set of positions in the sky, in order to monitor the variations of the night-sky brightness along the time at a particular location in the sky. The size of the sampled region around each position is defined by the user. Once selected, the program derives the mode of the night-sky surface brightness within this region, and stores it in a pre-defined ASCII file, for each acquired frame. The universal time is also stored in this file, to facilitate any possible long-term study of the light pollution at different locations in the sky.

4. RESULTS FROM THE CALIBRATION RUN

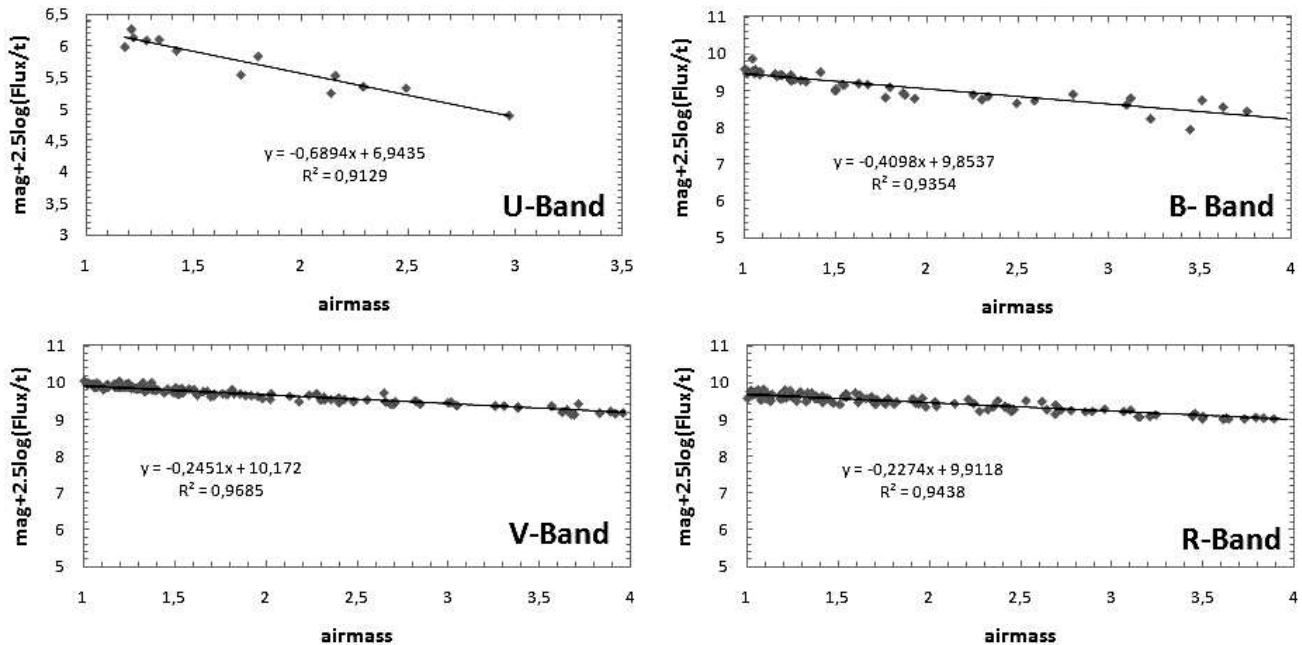


FIG. 8.— Example of the linear regression technique used to derive both the zero-point and the average extinction at a certain time for a considered filter. Each panel shows the distribution of the observed apparent magnitude versus the corresponding airmass for four of the five filters installed in the instrument: U, B, V and R-band. The data corresponds to the first calibration run with the instrument at the Calar Alto observatory. The number of stars detected per filter is considerably different, being 15, 57, 133 and 125, respectively. In this first calibration run only the stars brighter than 4 magnitudes in the V-band were used.

TABLE 1
ZERO POINTS FOR THE U, B, V, AND I JOHNSON BANDS

U	6.87 ± 0.15
B	9.889 ± 0.025
V	10.164 ± 0.011
R	9.906 ± 0.015
I	8.06 ± 0.21

A calibration run was performed during the photometric night of November 1st 2009, at the Calar Alto Observatory. The main goal of this calibration run was to obtain the finally required master calibration frames, derive the instrumental zero-points for the different bands and gather preliminary data to compare the results with previously reported ones.

4.1. A new approach to get flat fields

To obtain accurate flat field frames with a fisheye device is difficult due to the complexity of illuminating 180 degrees with an uniform light source. We designed an innovative procedure to obtain such flat field frames based on a uniform whitened dome, internally shined by a ring of white leds, located around the dome, at its bottom. A white ring located on top of the leds scatters the light within the dome, and produces the uniform illumination. A picture of this device, so-called DomeLight, is shown in Figure 5.

The uniformity of the inner illumination can be checked with the help of a CCD equipped with two small apertures faced up, near one to each other. This device allows us to sample small areas of the dome, while the contamination of the scattered light is minimized. The flux is measured at different locations within the dome

with the help of this device. No dependency is found along the different azimuthal angles, within a dispersion of just $\sim 5\%$. This dispersion corresponds to an error of less than 0.005 magnitudes in the derivation of the night-sky brightness, what has been considered in the error budget. On the other hand, it is seen a clear radial dependency of the illumination, that can be modelled by a simple second order polynomial function. This illumination correction is applied in the derivation of the flat field obtained with this device.

Figure 6 shows the radial and azimuthal distributions of the illumination, as derived on the basis of the procedure described before. An example of the typical flat-field frame obtained prior to the illumination correction is shown Figure 7.

Finally, the flatfield is derived by placing the DomeLight device on top of the protection transparent dome of the instrument. The sizes of both domes are calculated in such a way that they match each other. A set of exposures is taken with the lights of the DomeLight switched on. After applying the illumination correction a high quality master flat-field is derived. This master flat-field is stored to be used in any further reduction analysis.

4.2. Instrumental zero-point

Following the procedures described Section 2, once a frame is obtained for a particular band, the reduction procedure corrects it for the bias, the dark current and the flat-field. The astrometric solution is applied to the frame, and, according to the time and date, an automatic routine (similar to the one used to derive the astrometric solution) cross-checks the expected location of the stars in the photometric catalogue (Ducati 2002), and looks for

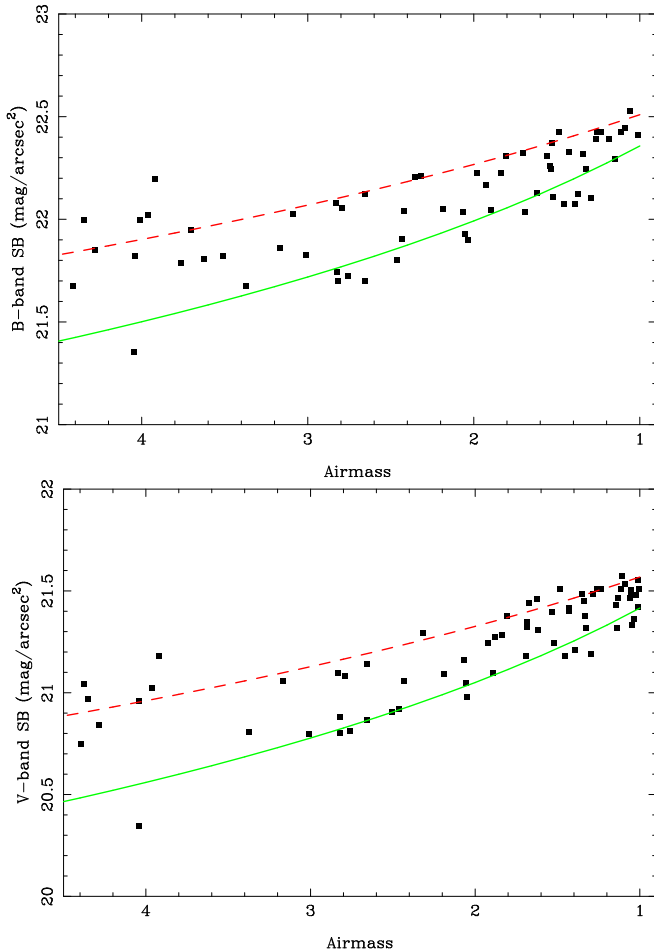


FIG. 9.— Distribution of the night sky surface brightness versus airmass for two of the five filters installed in the instrument: the B-band (top panel) and the V-band (bottom panel). The red dashed-line shows the expected distribution in the absence of light pollution, while the green solid-line shows the distribution when a $\sim 15\%$ of light pollution is taken into account.

nearby bright stars. Finally, following the aperture photometry technique described before, the program derives a final catalogue with the positions, airmasses, apparent magnitudes of the clearly identified stars, and the corresponding extinction at the considered location.

A new zero point is derived automatically for every single exposure, and the master value is updated if the atmospheric conditions are the proper ones. To do so, the software estimates the average extinction from the individual values derived at the location of each star. A clipping algorithm is applied to reject those values different in more than a 10% from the median value. If more than a 75% of the stars are within a 10% of the median value, the data are fitted adopting a linear regression based on Equation 1. If the correlation coefficient of this regression is larger than 0.95, the master zero point of the considered filter is automatically updated. If not, the average extinction is provided but it is not taken as a reference.

Figure 8 illustrates this process. In each panel of the figure it is shown the distribution of the apparent magnitude versus the airmass for four of the five filters installed in the instrument. Only the stars following the previously described rejection criteria are included in these

TABLE 2
COMPARISON OF THE EXTINCTION COEFFICIENTS

Band	CAHA	ASTMON
	κ_λ	κ_λ
B	0.27 ± 0.10	0.25 ± 0.03
V	0.18 ± 0.07	0.16 ± 0.08
I	0.08 ± 0.05	0.11 ± 0.01

figures. The solid line shows the result of the linear regression process for the plotted data points. Table 1 lists the values of the zero-points derived in the first calibration run, at the Calar Alto observatory.

In addition to the zero-point, the calibration procedure provides with an estimation of the global atmospheric extinction. However, while the zero-point is quite stable, the extinction is a highly variable parameter. Table 2 shows the comparison between the extinction coefficients published by Sánchez et al. (2007) for the Calar Alto observatory, and those derived by ASTMON along the Calibration Run in the night of the June 2nd, 2010, what was found to be mostly photometric. Both estimations of the average extinction are consistent one each other, showing that the instrument provides reliable measurements of this parameter. The simultaneous derivation of the extinction at different bands is required to analyze the relative contribution of different components to this extinction (scattering, dust attenuation and ozone absorption), which we will analyze in forthcoming studies, once we have collected an statistically significant number of data.

Figure 9 shows the distribution of the night-sky surface brightness derived by the instrument during the calibration run. The red dashed-line represents the expected night-sky surface brightness when no light pollution is considered. This red dashed-line has been derived assuming the airmass dependency of the natural night-sky surface brightness described in Benn & Ellison (1998a,b) and Sánchez et al. (2007,2008). The green solid line represents the expected night-sky surface brightness assuming a contribution of the light pollution of a 15% of the total night-sky surface brightness at the Zenith and assuming that it increases linearly with the airmass. We still do not know how the light pollution increases with the airmass, and therefore, this is the first attempt to model this distribution. However, it is found that the measured values are capped between both curves, and therefore, the contamination for the light pollution should not be larger than the estimated value. This value is of the order of the one reported by Sánchez et al. (2007), on the basis of the analysis of the night-sky spectrum at the observatory.

Many of the values reported on the night sky surface brightness published so far are based in a few amount of values (eg., Sánchez et al. 2007), and/or they have been taken with different instruments using different techniques since they were not the main goal of the observational projects (eg., Benn & Ellison et al. 1998a,b), which introduced errors difficult to control. The instrument described in this article is able to obtain a large number of estimations of the night sky surface brightness along a single night, taken on purpose, and easy to compare. With one acquisition per filter every minute, and a gap of 300 seconds per filter set, the instrument

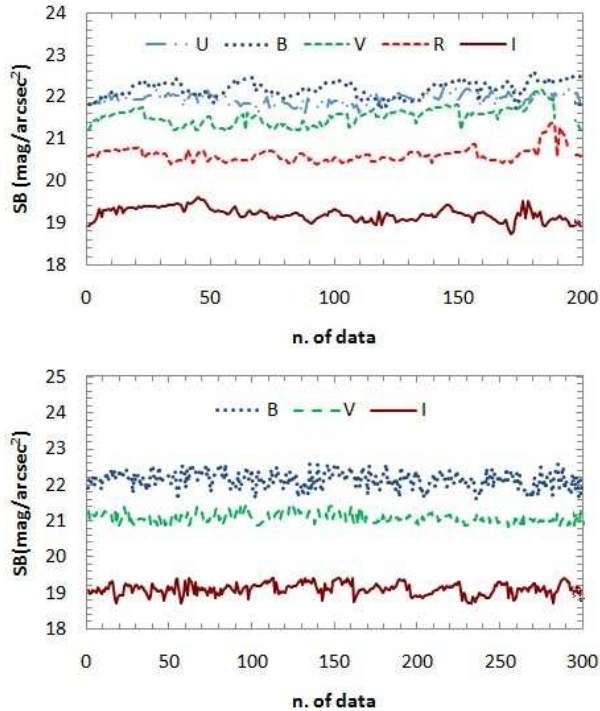


FIG. 10.— Monitoring of the night-sky surface brightness at the zenith for a complete month. Upper panel: data obtained at the Calar Alto observatory during January of 2011. Lower panel: data obtained at the Doñana National Park during May of 2010.

is able to complete a filter set (five filters) in ~ 8 minutes. Therefore, it provides ~ 75 individual estimations of the night-sky surface brightness per filter and night. With this amount of data it is possible to trace variations of the night-sky brightness along each night. Figure 10 shows an example of this monitoring process. The figure shows a comparison of the variation of the night-sky surface brightness at the zenith, monitored along a complete month, for the two locations where we have currently installed an ASTMON unit, the Calar Alto Observatory and the Doñana National Park. The data produced by long-term monitorings, similar to the presented in this figure but expanded along several years, will allow us to determine the differences in the night-sky brightness and spectral energy distribution at different locations, evaluating the seasonal and yearly evolution, and their dependency with other parameters (like the solar activity). We will have to acquire data for at least two years before deriving a firm conclusion about the seasonal evolution of the night-sky surface brightness, and for a period of more than eleven years to determine the effects of the solar activity.

The night-sky surface brightness is one of the parameters that qualifies better an astronomical site. In Sánchez et al. (2007) it was found that Calar Alto was among the best astronomical sites in the world, regarding this parameter. To provide a fair comparison, it is required to measure the night-sky brightness at the zenith, corrected for extinction and in a dark night (eg; Benn & Ellison 1998a,b). Table 3 shows the comparison between the values derived for the night-sky brightness using ASTMON during all the available dark time in a complete month (seeing in Figure 10), and those reported in the literature

TABLE 3
COMPARISON OF THE NIGHT-SKY SURFACE BRIGHTNESS

Band	ASTMON-Calar Alto *	ASTMON-Doñana **	CAHA***
U	22.02 ± 0.19	-	21.81 ± 0.10
B	22.29 ± 0.20	21.89 ± 0.3	22.41 ± 0.15
V	21.54 ± 0.10	20.95 ± 0.15	21.53 ± 0.18
R	20.59 ± 0.15	-	20.84 ± 0.27
I	19.11 ± 0.23	19.09 ± 0.25	18.70 ± 0.85

* Data obtained at Calar Alto Observatory during all the available dark time in January 2011.

** Data obtained at the Doñana National Park during all the available dark time in May 2010.

*** Data from the darkest night presented by Sánchez et al. (2007).

(Sánchez et al. 2007). The values are almost identical for any of the considered bands. The small discrepancies may be done due to the different seasons when the data were collected.

Figure 12 shows a typical example of the results obtained by ASTMON during a normal working sequence. The skybrightness maps were obtained in July 2010 at the Calar Alto night skies. The lower row displays the raw images while the upper one displays a colored sky brightness surface for the available sequence of filter (B, V, and I are shown in the figure). Each color represents different magnitudes per squared arcseconds and at a first sight the brightness variances of the sky can be easily identified.

For a quantitative inspection of the mentioned variances, the pixel's values of the FITS files contain the skybrightness value expressed in the appropriate units (i.e. magnitudes per squared arcseconds). This permits to display profiles along the frame. Figure 13 shows a particular example about the influence of the light pollution of a village being compared with the skybrightness value at the zenith. This will allow to perform detailed studies about the evolution in time, of the light pollution produced by the surrounding areas where ASTMON is located. A more detailed study of skybrightness in the areas mentioned in this paper will be prepared in a near future.

5. SUMMARY AND CONCLUSIONS

We have developed and manufactured the first permanent station to derive an exhaustive study of the light pollution and the atmospheric extinction, by applying the standard techniques of astronomical photometry. The system is based on a all-sky fisheye lens, with a filter wheel, and a CCD detector that allows to obtain automatic measurements of the night-sky surface brightness in 5 different bands. The system has been designed to afford extreme weather conditions and it can be installed in a remote place, being fully robotic. The instrument comprises a software that it is fully automatic. It performs all the required tools to operate the instrument, switching on and off automatically, acquires the science frames in the corresponding filters, and finally, reduces, calibrates and analyzes them to derive time dependent maps of the night-sky surface brightness, and individual estimations of atmospheric extinction for every band, together with a rough estimation of the cloud coverage.

The early experiments performed during the calibration runs of the instrument have demonstrated the valid-

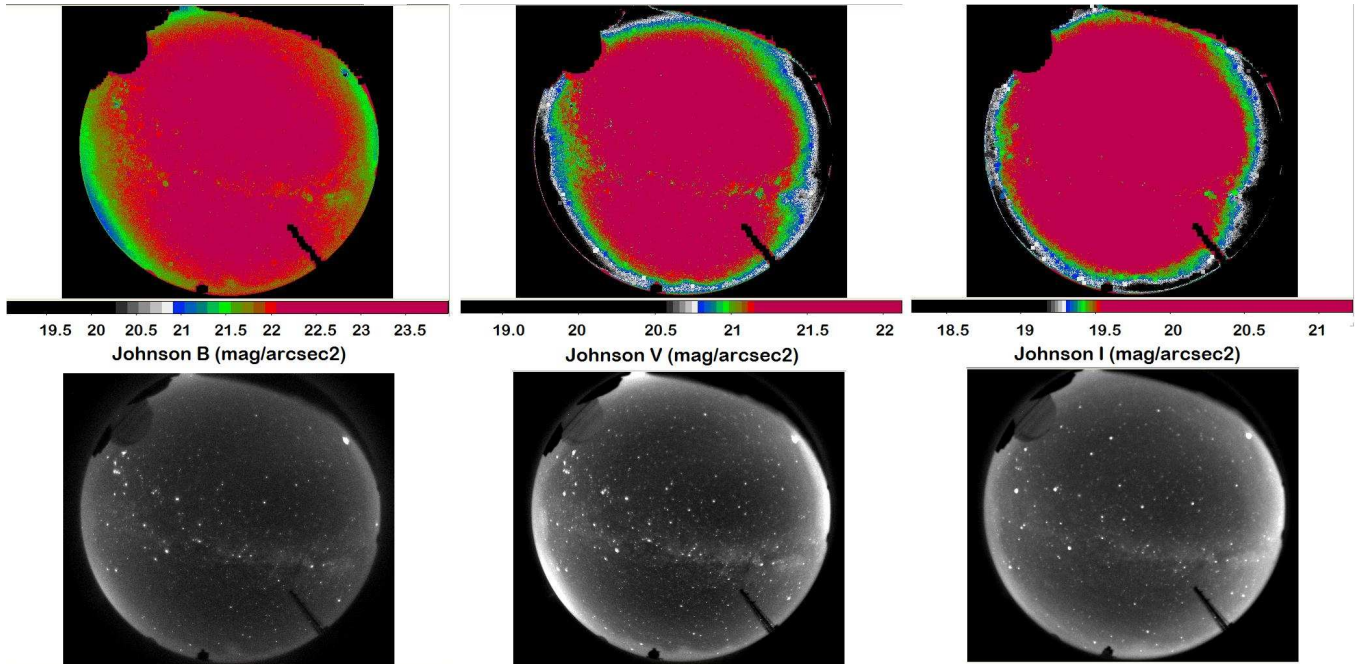


FIG. 11.— The final result of ASTMON is to provide a completely processed sky brightness map sequence of the whole sky for all the available filters as it is shown in this figure. Upper panel: Processed sequence. Each color represents different skybrightness level. Lower panel: Raw images. Data obtained by ASTMON at the Calar Alto observatory during July of 2010.

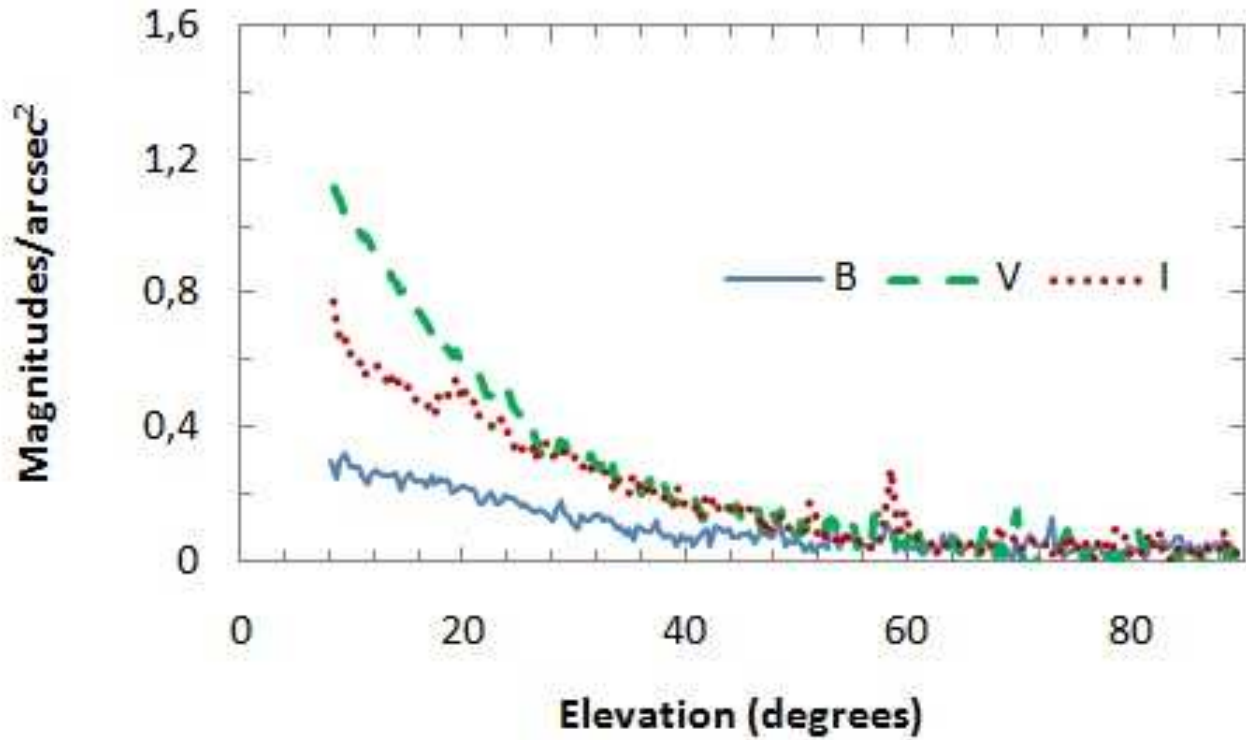


FIG. 12.— This figure shows the profile's variation of the zenith skybrightness to the horizon level affected by the light pollution of the near village Matalascañas in Huelva (Spain). Data obtained in December of 2010 at the Doñana National Park (Huelva).

ity of the conceptual design and its implementation. The values provided by the instrument, for both the night-sky surface brightness at the zenith, and the dust extinction, are consistent with ones reported in previous published results.

Currently, three ASTMON units have been installed at different locations in Spain: (i) the Calar Alto Observatory (Almeria); (ii) the Doñana National Park (Huelva) and (iii) the building of the Physics Department of the Universidad Complutense de Madrid (Madrid). All of them are fully operational and they are providing data for every clear night. A deep analysis of these data will be

presented in forthcoming articles, once we have acquired a statistically significant number of them.

6. ACKNOWLEDGMENTS

JA and SFS thanks the sub-programs of *Viabilidad, Diseño, Acceso y Mejora de ICTS*, ICTS-2008-24 and ICTS-2009-32, the *PAI Proyecto de Excelencia* P08-FWM-04319 and the funds of the PAI research group FQM360, and the MICINN program AYA2010-22111-C03-03.

REFERENCES

- Aceituno, J., 2004, Calar Alto Newsletter n.8, <http://www.caha.es/newsletter/news04b/Aceituno/Newsletter.html>
- Benn, C.R., Ellison, S.L., 1998, La Palma Technical Note, 115.
- Benn, C. R., & Ellison, S. L. 1998, *New Astronomy Review*, 42, 503
- Ducati, J. R. 2002, *VizieR Online Data Catalog*, 2237, 0
- High, F. W., Stubbs, C. W., Stalder, B., Gilmore, D. K., & Tonry, J. L. 2010, *PASP*, 122, 722
- Moles, M., et al. 2008, *AJ*, 136, 1325
- Moles, M., Sánchez, S. F., Lamadrid, J. L., Cenarro, A. J., Cristóbal-Hornillos, D., Maicas, N., & Aceituno, J. 2010, *PASP*, 122, 363
- Pérez-Rámirez, D., Aceituno, J., Ruiz, B., Olmo, F.J. and Alados-Arboledas, L., 2008, *Atmospheric Environment*, 42, 2733.
- Sánchez, S. F., Aceituno, J., Thiele, U., Pérez-Ramírez, D., & Alves, J. 2007, *PASP*, 119, 1186
- Sánchez, S. F., Thiele, U., Aceituno, J., Cristobal, D., Perea, J., & Alves, J. 2008, *PASP*, 120, 1244
- Zou, H., et al. 2010, *AJ*, 140, 602